SCIENCE CHINA
Information Sciences

• RESEARCH PAPER •

March 2025, Vol. 68, Iss. 3, 132202:1–132202:22
https://doi.org/10.1007/s11432-023-4285-3

Trajectory planning and tracking control for vehicles with tire blowout in complex traffic flows

Dongsheng YANG[1,2†], Di LIU[2†], Bing HAN[2], Guoxiang LU[2], Lingan KONG[2], Chaosheng HUANG[1] & Jun LI[1*]

[1]*School of Vehicle and Mobility, Tsinghua University, Beijing 100084, China*
[2]*BYD Auto Industry Company Limited, Shenzhen 518111, China*

Received 7 October 2023/Revised 18 June 2024/Accepted 18 August 2024/Published online 13 February 2025

Abstract This article focuses on the trajectory planning and tracking control of autonomous vehicles with tire blowouts in complex traffic flows. First, a lane change decision method for obstacle avoidance is developed based on coordinate system transformation projection. Second, combining this decision method, a lattice algorithm is developed with the kinematic constraint of the vehicle with a tire blowout to plan the trajectory in real-time. Third, the trajectory tracking control is decoupled longitudinally and laterally in the Frenet coordinate system. The existence of the optimal solution can be ensured by constructing a longitudinal speed control optimization problem and solving explicitly based on the Pontryagin maximum principle. Lateral displacement control problems are constructed and solved quickly by using the back-stepping method, in which Lyapunov stability can be demonstrated. Finally, the effectiveness of the proposed methods was verified through co-simulation.

Keywords complex traffic, trajectory planning, domain transformation decoupling, quick solution, tire blowout

Citation Yang D S, Liu D, Han B, et al. Trajectory planning and tracking control for vehicles with tire blowout in complex traffic flows. Sci China Inf Sci, 2025, 68(3): 132202, https://doi.org/10.1007/s11432-023-4285-3

1 Introduction

Due to the various traffic elements in the driving environment of autonomous vehicles, their dynamic characteristics make the task of ensuring safety and comfort huge and complex. Aiming to ensure vehicle operation safety when obstacles appear, autonomous vehicles need to re-plan their trajectories based on obstacle information in the local time domain, meanwhile, the overall trend is to track global trajectory in the distance domain. In the local planning process, it is not only necessary to consider the constraints brought by real-time traffic environment on vehicle movement, but also the safety of vehicles and the optimality of driving tasks.

Research has found that in complex traffic flows, errors after a tire blowout, delayed vehicle response or operations are the main causes of accidents [1]. Therefore, there is an urgent need for active safety control of tire blowout vehicles. Researches mainly focus on the stability control of vehicles after tire blowout based on the prediction of the vehicle state [2–4]. With the development of autonomous driving technology and networking technology, trajectory planning and tracking, as important components of autonomous driving, have been widely studied. This provides an important theoretical reference for the study of autonomous vehicles automatically changing from the current lane to the emergency lane after a tire blowout. The existing research is mainly based on trajectory planning based on the self running state in the Cartesian coordinate system [5–8]. It is necessary to plan the real-time trajectory of the vehicle in consideration of the complex traffic environment and the kinematics constraints brought by tire blowouts to ensure driving safety.

According to the different principles used, trajectory planning algorithms can be divided into search-based algorithms, sampling based algorithms, intelligent algorithms and learning-based algorithms [9]. Search-based algorithms mainly include the A* algorithm [10, 11], depth first search (DFS) algorithm

* Corresponding author (email: lijun1958@tsinghua.edu.cn)
† These authors contributed equally to this work.

[12–14], and breadth first search (BFS) algorithm [15]. These algorithms are based on global information for searching and are suitable for static planning. Intelligent algorithms mainly include the ant colony algorithm [16,17], which can quickly solve problems in parallel but produces random optimization results; the back propagation (BP) algorithm [18, 19], which can handle nonlinear problems well but easily falls into local minima; and the rapidly-exploring random tree (RRT) algorithm [20–22], which can handle path planning problems well with non-holonomic constraints, although the optimal solution is not necessarily obtained. Learning-based algorithms mainly include the deep Q-network (DQN) algorithm [23–25], which has strong versatility but cannot be applied to continuous control scenarios, and the deep deterministic policy gradient (DDPG) algorithm [26, 27], which produces a stable solution but is not applicable to dynamic random scenarios. The deep reinforcement learning algorithm relies on the learning ability of the hardware, and it is an end-to-end method, for which it is difficult to make the planning and decision-making process clear. Comparing these algorithms, it is found that traditional quintic polynomial algorithms exhibit good adaptability and smoothness and are easier to implement.

After planning the local obstacle avoidance trajectory, vehicle motion control is the key part of the autonomous vehicle decision-planning-control architecture. The essence of trajectory tracking control is to ensure that the autonomous vehicle follows the planned trajectory as closely as possible while ensuring stability and safety; meanwhile, the corresponding control parameters are sent to the actuator, such as the front wheel deviation and wheel braking forces.

Traditional control methods are widely used due to their simplicity and stability; these include proportional-integral-derivative (PID) control [28,29], sliding mode control [30–32], preview control [33,34], and fuzzy control [35]. PID control is simple, reliable and easy to implement, but the parameters are difficult to determine. Preview control is suitable for tracking control under multiple working conditions, but it is prone to fluctuations when the preview point error is large, and its robustness to common disturbances is poor. Sliding mode control has strong anti-interference ability and good robustness but is prone to chattering.

With the development of control theories, methods based on optimal control algorithms and intelligent algorithms have emerged, mainly including model predictive control (MPC) [36, 37], neural networks (NNs) [38,39], and reinforcement learning (RL) [40,41]. MPC can easily handle multiple constraints and states in multiobjective optimization, but its real-time performance is poor. The construction of NNs, RL and other methods for solving such problems is complex, as they have a large computational workload and parameters that are difficult to adjust. In practical applications, due to the good ability of MPC to handle multistate and multiconstraint problems, most researchers still use the improved MPC method in trajectory tracking research.

Existing optimization based methods make it difficult to obtain the optimal trajectory if the fragile stable state of the vehicle with tire blowout is considered. However, if the vehicle state is not considered, the planned trajectory is not executable or may cause instability. Existing enumeration based planning methods can obtain the optimal trajectory of a vehicle with tire blowout by comparing trajectories one by one, but they require a large amount of computation and are not suitable quickly respond for vehicles with tire blowout.

Aiming at planning a safe and silky obstacle avoidance trajectory for vehicles with a tire blowout, and controlling the vehicles to follow this trajectory, this paper discusses how to use surrounding vehicle information to reduce the computational complexity of the lattice algorithm, and presents a real-time explicit control algorithm based on the Pontryagin maximum principle (PMP), which can be implemented in hardware. The contributions of this research include the following aspects. Using surrounding vehicle information to pre-determine the feasible obstacle avoidance area for the lattice method to plan trajectories. Incorporating lateral and longitudinal acceleration jerk constraints in the planning makes the trajectory more friendly to the stable operation of vehicles after a tire blowout. The Hamiltonian function is constructed according to the PMP. The original optimization problem is transformed into solving the optimal initial value of the covariant variable in the Hamiltonian function. Then, the explicit control sequence of the optimization problem can be obtained recursively.

The overall research structure is shown in Figure 1. First, the state of the surrounding road is obtained, and the global initial reference trajectory is planned. Second, based on the status of vehicles in the surrounding lanes, the lanes available for avoiding obstacles are determined. Then, considering the lane availability, trajectory planning is conducted for obstacle avoidance, and the obstacle avoidance trajectory is transformed into the Frenet coordinate system. Finally, the longitudinal speed control optimization problem and the lateral heading control problem are constructed separately. Within the framework of

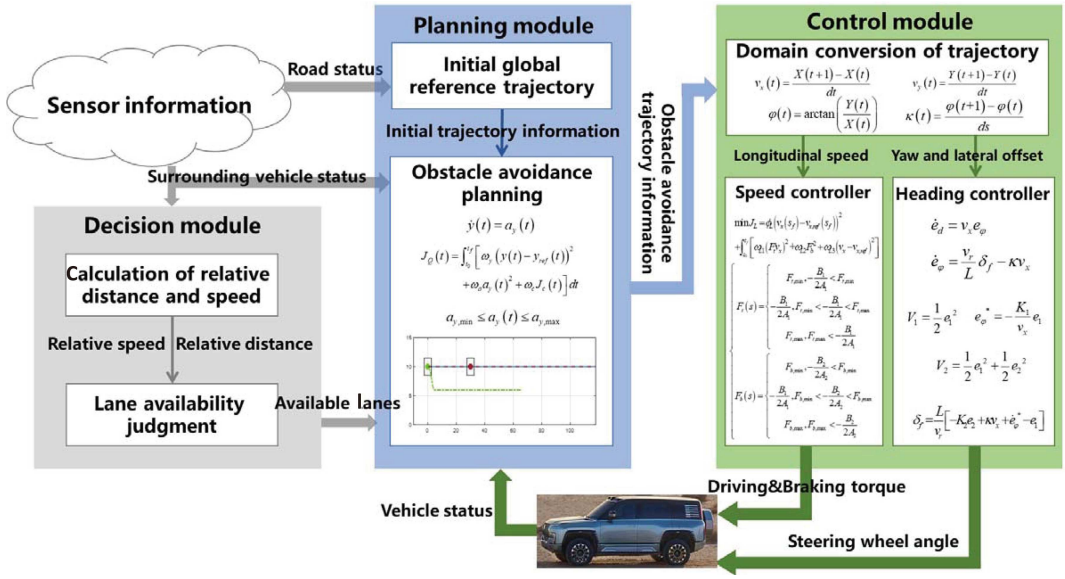

Figure 1 (Color online) Overall research structure.

MPC, the PMP is used to quickly solve the longitudinal speed control optimization problem, and the existence of the optimal solution is proved. The explicit expression of the optimal control commands for solving the lateral heading control optimization problem is derived using the back-stepping method, and the Lyapunov stability of the proposed method is demonstrated.

2 Lane change decision and obstacle avoidance trajectory planning for vehicles with tire blowout

2.1 Lane availability decision

When a vehicle experiences a tire blowout, it is necessary to plan a global initial reference trajectory to reach a safe location where the vehicle can stop so that the tire blowout can be addressed. Therefore, the centerline of the low-speed lane is taken as the initial global reference trajectory.

Based on vehicle-vehicle, vehicle-road and vehicle-sensor information, the system determines whether lane changing can be implemented. If the opportunity for lane changing is available, the vehicle implements lane change trajectory planning and tracking. Otherwise, the vehicle maintains the current route. If the current lane conditions are unsafe, the vehicle directly performs emergency braking. The main methods for making lane change decisions include rule-based methods [42], cognitive methods [43], and learning methods [44]. Due to the instability of vehicles with flat tires, the availability of alternative lanes needs to be quickly determined. Therefore, this article presents an improved lattice method with the ability to make rapid lane-changing decisions and perform vehicle status analysis.

The left lane of the ego-vehicle (EV) is chosen to define the available lane. At time t, the vehicle with the tire blowout is located in. When encountering obstacles that must be avoided, the EV will have different potential trajectories, as shown in Figure 2, including acceleration to change lanes (as shown by the red line), changing lanes at a constant speed (as shown by the light red line), and deceleration to change lanes (as shown by the yellow line). Regardless of which trajectory is chosen, the EV must maintain safe conditions considering surrounding vehicles. Therefore, these potential trajectories are selected by incorporating the safety distance between vehicles. Vehicle lateral motion is dependent on longitudinal motion in the Cartesian coordinate system, but in the Frenet coordinate system, the lateral and longitudinal motion of the vehicle can be decoupled; therefore, the coordinates are translated from the Cartesian system to the Frenet system to determine lane availability, as shown in Figure 2 ①. After projecting onto the same lane, the available trajectory for vehicle obstacle avoidance changes from the four possible positions in Figure 2 ① to the two possible positions in Figure 2 ②.

A cluster of possible trajectories that need further analysis will be generated, as shown in Figure 2 ③. It is necessary to make judgments based on the longitudinal speed, acceleration, and position of

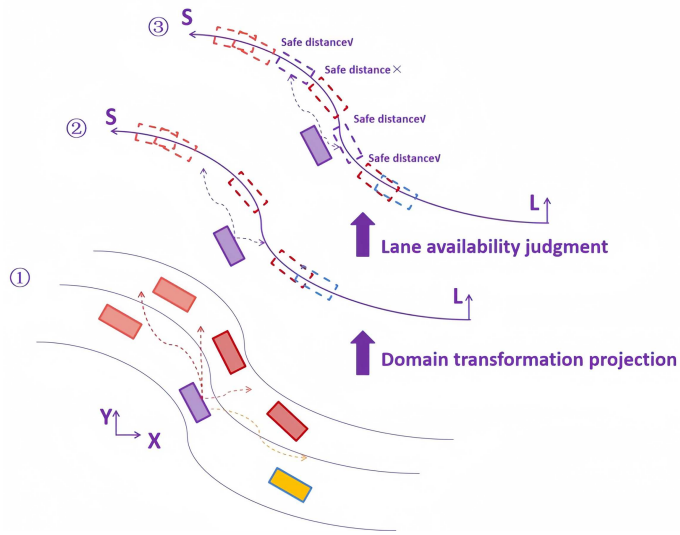

Figure 2 (Color online) Schematic of lane availability judgment.

the EV and obstacle-vehicles (OVs). In the Frenet coordinate system, only the longitudinal motion of the vehicle needs to be considered. Therefore, the S-coordinate, speed and acceleration of the EV are defined as $\{S_e(t), v_e(t), a_e(t)\}$, and the S-coordinate, speed and acceleration of the OVs are defined as $\{S_i(t), v_i(t), a_i(t)\}$, where $i = 1, 2, \ldots, N$ are the numbers of the OVs. On the projection road, the distance between the EV projection and the front OV projection is d_{i-e}, the distance between the EV projection and the rear OV projection is d_{e-i+1}, and the distance between the i-th vehicle projection and the $(i+1)$-th vehicle projection is d_{i-i+1}. Then, when there is a lane change time t_d such that

$$v_i t + \frac{1}{2} a_i t^2 + d_{\text{safe}} \geqslant v_e t + \frac{1}{2} a_e t^2 \quad (i = 1, 2, \ldots, N), \tag{1}$$

the forward feasible obstacle avoidance entry position is d_{i-e}, and when

$$v_e t + \frac{1}{2} a_e t^2 + d_{\text{safe}} \geqslant v_i t + \frac{1}{2} a_i t^2 \quad (i = 1, 2, \ldots, N), \tag{2}$$

the backward feasible obstacle avoidance entry position for vehicles in the backward direction is d_{e-i+1}.

d_{i-i+1} is a feasible vehicle obstacle avoidance entry position when both d_{i-e} and d_{e-i+1} are determined simultaneously. When

$$D = d_{i-i+1} | i = 1, 2, \ldots, N = \emptyset, \tag{3}$$

lane Lane_{i+1} and Lane_{i-1} are the available lanes. Then, in obstacle avoidance trajectory planning, when Lane_{i+1} and Lane_{i-1} are available, either lane can be preferred as an obstacle avoidance lane. When there are no such lanes on either side, the original lane Lane_i is selected as the obstacle avoidance lane.

2.2 Obstacle avoidance trajectory combined with vehicle dynamic constraints

Because the slip of a vehicle during a turn is related to its longitudinal speed, slipping can be avoided with longitudinal speed control. However, the curvature of the real-time planned trajectory will affect the lateral acceleration of the vehicle during the turn, which determines whether the vehicle will roll over when tracking the obstacle avoidance trajectory. Therefore, it is necessary to consider the available lateral acceleration of the vehicle.

The overall obstacle avoidance strategy is for vehicles to track the global planned trajectory and only perform obstacle avoidance planning when obstacles appear on the global trajectory. Obstacle avoidance trajectory planning for automatic vehicles includes path generation, path optimization, and speed control. Path generation mainly calculates collision-free trajectories from the initial point to the target point, performing tasks such as state space sampling, collision detection, and obstacle avoidance. Path optimization mainly calculates trajectories that comply with vehicle integrity constraints among multiple trajectories, and it improves the smoothness of these trajectories through spline interpolation

algorithms. Speed planning includes the calculation of linear and angular velocities at which the EV will not collide with any OVs. The input of motion planning is the terminal state provided by the positioning system and the environment description provided by the perception system. Through the three steps of motion planning, a smooth trajectory satisfying the constraints of the intelligent vehicle is ultimately output.

In this paper, the lattice obstacle avoidance algorithm is improved. Based on the state grid idea of the lattice algorithm, road decision-making and vehicle dynamic constraints are added. When dividing the status of the EV with a tire blowout into grids, to ensure stability during obstacle avoidance planning, the vehicle's longitudinal and lateral acceleration and jerk should be constrained to within a reasonable range, that is [45]

$$\begin{aligned}
&\ddot{s}_{\min}(t) \leqslant \ddot{s}_{\{0,T\}}(t) \leqslant \ddot{s}_{\max}(t),\\
&\ddot{d}_{\min}(t) \leqslant \ddot{d}_{\{0,T\}}(t) \leqslant \ddot{d}_{\max}(t),\\
&\dddot{s}_{\min}(t) \leqslant \dddot{s}_{\{0,T\}}(t) \leqslant \dddot{s}_{\max}(t),\\
&\dddot{d}_{\min}(t) \leqslant \dddot{d}_{\{0,T\}}(t) \leqslant \dddot{d}_{\max}(t),
\end{aligned} \quad t_0 \leqslant t \leqslant t_f, \tag{4}$$

where $\ddot{s}_{\min}(t)$, $\ddot{s}_{\max}(t)$, $\ddot{d}_{\min}(t)$ and $\ddot{d}_{\max}(t)$ are, respectively, the minimum longitudinal acceleration, maximum longitudinal acceleration, minimum lateral acceleration, and maximum lateral acceleration to ensure the stable and smooth driving of the EV with a tire blowout. $\dddot{s}_{\min}(t)$, $\dddot{s}_{\max}(t)$, $\dddot{d}_{\min}(t)$ and $\dddot{d}_{\max}(t)$ are the minimum longitudinal jerk, maximum longitudinal jerk, minimum lateral jerk, and maximum lateral jerk needed to ensure the stable and smooth driving of the EV with a tire blowout.

The traditional lattice algorithm arranges the vehicle's longitudinal and lateral distance, velocity, and acceleration in a grid within specified ranges. For each grid state, a fifth-degree polynomial is used to fit the obstacle avoidance trajectory, and then the collision costs between the trajectories and the OVs are determined to select the optimal obstacle avoidance trajectory [46]. This article aims to balance the traffic flow information and the dynamic constraints of the vehicle with tire blowout. Eqs. (1)–(4) are combined to update the ranges of the vehicle status grid in real time. Eqs. (1)–(3) are used to provide the lateral distance range combined with traffic information, and Eq. (4) provides the longitudinal speed and acceleration and the lateral speed and speed range.

A notable distinction is needed here. In the real world, the longitudinal distance, velocity, and acceleration are functions of time t, while the lateral distance compared to the global reference trajectory is a function of the longitudinal distance s.

$$\begin{pmatrix} s_0 \\ s_T \\ \dot{s}_0 \\ \dot{s}_T \\ \ddot{s}_0 \\ \ddot{s}_T \end{pmatrix} = \begin{pmatrix} 0 & 0 & 0 & 0 & 0 & 1 \\ T^5 & T^4 & T^3 & T^2 & T & 1 \\ 0 & 0 & 0 & 0 & 1 & 0 \\ 5T^4 & 4T^3 & 3T^2 & 2T & 1 & 0 \\ 0 & 0 & 0 & 2 & 0 & 0 \\ 20T^3 & 12T^2 & 6T & 2 & 0 & 0 \end{pmatrix} \begin{pmatrix} b_0 \\ b_1 \\ b_2 \\ b_3 \\ b_4 \\ b_5 \end{pmatrix}, \tag{5}$$

$$\begin{pmatrix} d_0 \\ d_s \\ \dot{d}_0 \\ \dot{d}_s \\ \ddot{d}_0 \\ \ddot{d}_s \end{pmatrix} = \begin{pmatrix} 0 & 0 & 0 & 0 & 0 & 1 \\ S^5 & S^4 & S^3 & S^2 & S^1 & 1 \\ 0 & 0 & 0 & 0 & 1 & 0 \\ 5S^4 & 4S^3 & 3S^2 & 2S^1 & 1 & 0 \\ 0 & 0 & 0 & 2 & 0 & 0 \\ 20S^3 & 12S^2 & 6S^1 & 2 & 0 & 0 \end{pmatrix} \begin{pmatrix} c_0 \\ c_1 \\ c_2 \\ c_3 \\ c_4 \\ c_5 \end{pmatrix}, \tag{6}$$

where c_i, b_i $(i = 1, 2, 3, 4, 5)$ are the fitting coefficients of the fifth-degree polynomial; s_0, $\dot{s}_0$ and $\ddot{s}_0$ are the longitudinal distance, speed, and acceleration given for the initial state; and d_0, $\dot{d}_0$ and $\ddot{d}_0$ are the lateral distance, velocity, and acceleration given for the initial state of the vehicle. s_T, $\dot{s}_T$ and $\ddot{s}_T$ are the longitudinal distance, speed, and acceleration of the vehicle in the terminal state according to (4); d_T, $\dot{d}_T$ and $\ddot{d}_T$ are the lateral distance, velocity, and acceleration of the vehicle in the terminal state according to (4).

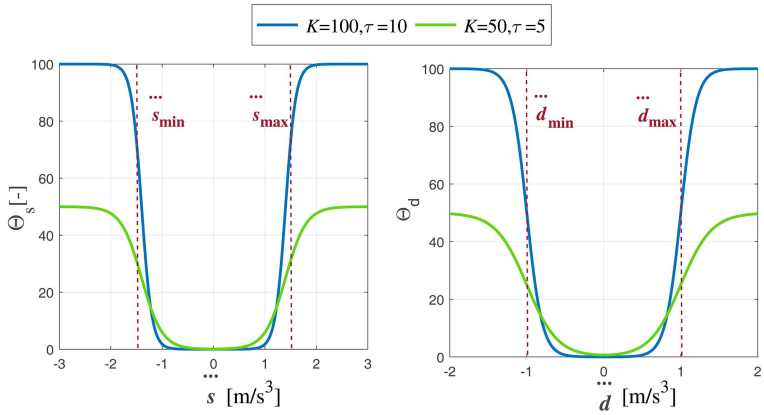

Figure 3 (Color online) Parameters of jerk cost function and corresponding function forms.

According to (5) and (6), a vehicle obstacle avoidance trajectory cluster that takes into account both traffic flow information and EV tire blowout dynamic constraints can be obtained. Since the states of OVs in the traffic flow constantly change and the EV with a tire blowout has acceleration constraints, it is necessary to further screen out collision avoidance trajectories that meet the acceleration constraints in (4) and combine the prediction of the EV state with the prediction of the OV states. The cost function for trajectory selection is

$$J=\sum_{i=1}^{N}\omega_c\left(\frac{(s_{\mathrm{OV}}-s)^2}{(L_{\mathrm{OV}}^2+\varepsilon_L)}+\frac{(d_{\mathrm{OV}}-d)^2}{(W_{\mathrm{OV}}^2+\varepsilon_W)}\right)+(\omega_{\mathrm{as}}\Theta_s+\omega_{\mathrm{ad}}\Theta_d), \tag{7}$$

where the first term is the cost function of collision detection with OV states that change over time; s_{OV} and d_{OV} are the longitudinal predicted distances of OVs; L_{OV} and W_{OV} are the length and width of the obstacle vehicles; and ϵ_L and ϵ_W are minimal supplementary parameters that prevent a zero denominator due to the target detection angle. ω_c, ω_{as} and ω_{ad} are the adjustment parameters of the cost function. The second and third terms are the cost functions for the lateral and longitudinal jerk constraints:

$$\Theta_s=\frac{K}{1+\mathrm{e}^{\tau\left(\dddot{s}_{\min}-\dddot{s}_{\{0,T\}}\right)}}+\frac{K}{1+\mathrm{e}^{\tau\left(\dddot{s}_{\{0,T\}}-\dddot{s}_{\max}\right)}}, \tag{8}$$

$$\Theta_d=\frac{K}{1+\mathrm{e}^{\tau\left(\dddot{d}_{\min}-\dddot{d}_{\{0,T\}}\right)}}+\frac{K}{1+\mathrm{e}^{\tau\left(\dddot{d}_{\{0,T\}}-\dddot{d}_{\max}\right)}}. \tag{9}$$

The setting of K will affect the maximum value of the cost, and the setting of τ will affect the smoothness of the penalty term on the allowed region boundary, as shown in Figure 3.

When EV and OVs are determined, their collision risk will also be determined. The second term of (7) is related to the kinematic constraints of the vehicle with a tire blowout. According to Figure 3, Eq. (7) is composed of a fixed value and a convex function, that is, the overall function is convex. When solving this convex function, the optimal value of (7) can be obtained by comparing (7) corresponding to each trajectory using the enumeration method.

In Lattice planning, the optimal solution is obtained by comparing the trajectories through the enumeration method. Because in vehicle trajectory planning, the first priority is to ensure collision safety, and the second thing is to ensure that the kinematic constraints of a tire blowout vehicle are met during operation, so in the experiments of this article, we set $\omega_{\mathrm{as}}=\omega_{\mathrm{ad}}$ in (7), and $10\leqslant\omega_c/\omega_{\mathrm{as}}\leqslant 10^2$.

According to the above definition and derivation, the trajectory satisfying the vehicle dynamic constraints can be obtained. Taking a straight road with no OVs ahead as an example, at the initial moment, the feasible distance range, speed range, and expected arrival time range of the current position in the Frenet coordinate system are gridded. Then, the feasible longitudinal trajectory clusters for each combination of grid nodes are calculated using (5).

After determining the trajectory of the longitudinal distance, the lateral distance range, lateral velocity range, and lateral acceleration range corresponding to the end point of each segment are gridded. According to (6), the lateral trajectory clusters corresponding to each segment are calculated.

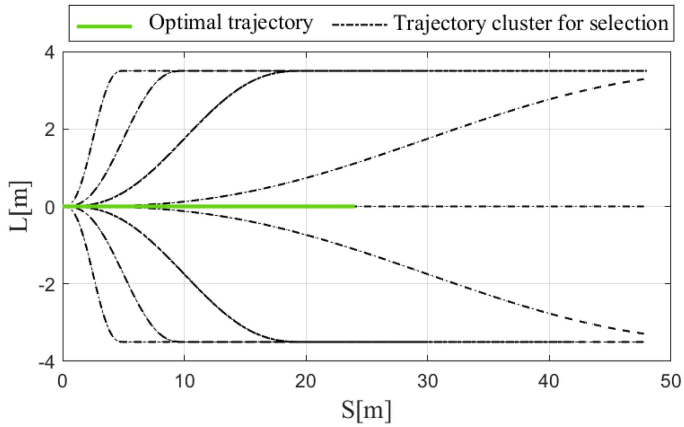

Figure 4 (Color online) Straight lane scene trajectory selection.

Combining the information of the EV and OVs with (7), trajectory clusters are selected to obtain the longitudinal and lateral trajectories that minimize cost function (7). The combination of these longitudinal and lateral trajectories is the real-time optimal trajectory, as shown in Figure 4. To facilitate the design of vehicle controllers, the trajectory data obtained from the planning method are preprocessed in the Frenet coordinate system; the velocity, curvature, and yaw angle of each data point are obtained; and the longitudinal speed controller and lateral controller of the vehicle are decoupled and designed.

2.3 Trajectory data conversion processing

The upper-level demand trajectory coordinate data (X, Y) from the Cartesian coordinate system are converted to the coordinate data (S, L) in the Frenet coordinate system, and the velocity, curvature, and yaw angle of each data point are calculated.

The longitudinal speed is calculated as

$$v_x(t) = \frac{X(t+1) - X(t)}{\mathrm{d}t}, \tag{10}$$

where t is the time. Therefore, $X(t)$ is the abscissa of the planned trajectory at time t, $X(t+1)$ is the abscissa of the planned trajectory at time $t+1$, and $\mathrm{d}t$ is the time interval of the data points obtained from the Cartesian coordinates.

The lateral velocity is calculated as

$$v_y(t) = \frac{Y(t+1) - Y(t)}{\mathrm{d}t}, \tag{11}$$

where $Y(t)$ is the ordinate of the planned trajectory at time t, and $Y(t+1)$ is the ordinate of the planned trajectory at time $t+1$.

The resultant velocity is

$$v_{\mathrm{ref}}(t) = \sqrt{v_x(t)^2 + v_y(t)^2}. \tag{12}$$

The yaw angle is

$$\varphi(t) = \arctan\left(\frac{Y(t)}{X(t)}\right). \tag{13}$$

The curvature is

$$\kappa(t) = \frac{\varphi(t+1) - \varphi(t)}{\mathrm{d}s}. \tag{14}$$

When the demand trajectory is known, the demand trajectory at an arbitrary time t corresponds to a fixed position s, and the conversion relationship between the unit time interval and unit distance interval is

$$\mathrm{d}t = \frac{\mathrm{d}s}{v(t)}. \tag{15}$$

3 Lateral and longitudinal control with vehicle trajectory tracking

3.1 Design of a longitudinal vehicle speed prediction controller based on Pontryagin's maximum principle

When only the longitudinal direction is considered, the longitudinal motion equation of the vehicle is constructed as follows:

$$\dot{v}_x(s) = \frac{F_t(s) - F_b(s)}{Mr} - g\sin(\theta) - C_r g\cos(\theta) - \frac{1}{2}A\rho C_f v_x(s)^2, \tag{16}$$

where $F_t(s)$ is the driving torque at the wheel, $F_b(s)$ is the braking torque at the wheel, M is the vehicle mass, r is the tire radius, g is the gravitational acceleration, θ is the road slope, C_r is the rolling friction coefficient, A is the windward area of the vehicle, ρ is the density of air, C_f is the wind resistance coefficient, $v(s)$ is the resultant speed at position s, and $\dot{v}_x(s)$ is the longitudinal acceleration. The vertical deceleration caused by gravity when the road slope is extremely small can be neglected; i.e., $g\sin(\theta) \approx 0$. Moreover, there are few vehicles in an urban area operating at high speeds, and the deceleration caused by wind resistance can be neglected; i.e., $\frac{1}{2}A\rho C_f v_x(s)^2 \approx 0$.

Because the safety of the vehicle with a tire blowout is taken into account in the decision and planning layers and the lane change decision is mainly related to lateral motion, additional optimization requirements can be taken into account when controlling the vehicle's longitudinal motion. When a vehicle with a tire blowout is operating, the safe trajectory should be accurately tracked, and the speed adjustment should be as small as possible to maintain stability. During safe obstacle avoidance operations, it is also expected that energy consumption will be reduced in response to the emergency situation. Based on the above requirements, the objective function is constructed as follows:

$$J_L = \phi_L(v_x(s_f) - v_{x,\mathrm{ref}}(s_f))^2 + \int_{s_0}^{s_f} \left[\omega_{L1}(F_t(s)v_x(s))^2 + \omega_{L2}F_b(s)^2 + \omega_{L3}(v_x(s) - v_{x,\mathrm{ref}}(s))^2\right] \mathrm{d}s, \tag{17}$$

where the first term optimizes energy consumption, the second term reduces braking to maintain stable vehicle speed, and the third term tracks the planned trajectory. J_L is the objective function for longitudinal vehicle control, ϕ_L is the weight of the longitudinal vehicle control terminal constraint, s_f is the predicted terminal position in the Frenet coordinate system, s_0 is the predicted starting position in the Frenet coordinate system, ω_{L1} is the energy consumption optimization weight, ω_{L2} is the comfort optimization weight, ω_{L3} is the longitudinal speed tracking optimization weight, and $v_{x,\mathrm{ref}}(s)$ is the longitudinal speed of the planned trajectory at position s.

Because the performance of a vehicle with a tire blowout is different from that of a normal vehicle, it is necessary to give a performance constraint for both the driving torque and braking torque according to the vehicle dynamic characteristics. Therefore, the control input constraints of the optimization problem are

$$F_{t,\min} \leqslant F_t(s) \leqslant F_{t,\max}, \tag{18}$$

$$F_{b,\min} \leqslant F_b(s) \leqslant F_{b,\max}, \tag{19}$$

where $F_{t,\min}$ is the minimum driving torque, $F_{t,\max}$ is the maximum driving torque, $F_{b,\min}$ is the minimum braking torque, and $F_{b,\max}$ is the maximum braking torque.

In summary, the longitudinal optimization problem for vehicles with a tire blowout is as follows:

$$\begin{aligned}
&\min\ J_L = \phi_L(v_x(s_f) - v_{x,\mathrm{ref}}(s_f))^2 + \int_{s_0}^{s_f} \left[\omega_{L1}(F_t(s)v_x(s)) + \omega_{L2}F_b(s)^2 + \omega_{L3}(v_x(s) - v_{x,\mathrm{ref}}(s))^2\right] \mathrm{d}s\\
&\text{s.t. } \dot{v}_x(s) = \frac{F_t(s) - F_b(s)}{Mr} - g\sin(\theta) - C_r g\cos(\theta) - \frac{1}{2}A\rho C_f v_x(s)^2,\\
&\quad F_{t,\min} \leqslant F_t(s) \leqslant F_{t,\max},\\
&\quad F_{b,\min} \leqslant F_b(s) \leqslant F_{b,\max}.
\end{aligned} \tag{20}$$

At high speeds and in traffic flows, to achieve safe and accurate control of a vehicle, it is necessary to quickly solve optimization problem (20). The existing methods for solving optimization problems are mostly numerical iterative methods, which require a large amount of computation, resulting in a slow

calculation speed. The method of this article is based on the PMP and uses indirect methods to quickly solve optimization problems.

First, a Hamiltonian function is constructed based on the PMP

$$\begin{aligned}&H\left(v_x(s),F_t(s),F_b(s),\lambda(s)\right)\\&=\left[\omega_{L1}(F_t(s)v_x(s))^2+\omega_{L2}F_b(s)^2+\omega_{L3}(v_x(s)-v_{x,\mathrm{ref}}(s))^2\right]+\lambda(s)\left[\frac{F_t(s)-F_b(s)}{Mr}-C_rg\cos(\theta)\right],\end{aligned}\tag{21}$$

where $\lambda(s)$ is the covariate variable. The canonical equation for obtaining the optimal solution is

$$\dot{\lambda}(s)=-\frac{\partial H\left(v_x(s),F_t(s),F_b(s),\lambda(s)\right)}{\partial v_x(s)}=-\left[2\omega_{L1}F_t(s)^2v_x(s)+2\omega_{L3}\left(v_x(s)-v_{x,\mathrm{ref}}(s)\right)\right].\tag{22}$$

The cut-off condition for predicting terminals is

$$\lambda\left(s_f\right)-2\phi_L\left(v_x\left(s_f\right)-v_{x,\mathrm{ref}}\left(s_f\right)\right)=0.\tag{23}$$

Rewriting the Hamiltonian function in the functional form of control variables yields

$$\begin{aligned}&H\left(v_x(s),F_t(s),F_b(s),\lambda(s)\right)\\&=\omega_{L1}v_x(s)^2F_t(s)^2+\lambda(s)\frac{F_t(s)}{Mr}+\omega_{L2}F_b(s)^2-\lambda(s)\frac{F_b(s)}{Mr}+\omega_{L3}(v_x(s)-v_{x,\mathrm{ref}}(s))^2-C_rg\cos(\theta).\end{aligned}\tag{24}$$

We define

$$\begin{aligned}&A_1=\omega_{L1}v_x(s)^2,\\&B_1=\frac{\lambda(s)}{Mr},\\&A_2=\omega_{L2},\\&B_2=-\frac{\lambda(s)}{Mr},\\&C=\omega_{L3}(v_x(s)-v_{x,\mathrm{ref}}(s))^2-C_rg\cos(\theta).\end{aligned}\tag{25}$$

Since the driving torque $F_t(s)$ and braking torque $F_b(s)$ cannot be nonzero simultaneously, the driving torque and braking torque that minimize the Hamiltonian function can be obtained by determining the optimal value of the quadratic function

$$\begin{cases}F_t(s)=\begin{cases}F_{t,\min},-\dfrac{B_1}{2A_1}<F_{t,\min},\\-\dfrac{B_1}{2A_1},F_{t,\min}<-\dfrac{B_1}{2A_1}<F_{t,\max},\\F_{t,\max},F_{t,\max}<-\dfrac{B_1}{2A_1},\end{cases}\\F_b(s)=\begin{cases}F_{b,\min},-\dfrac{B_2}{2A_2}<F_{b,\min},\\-\dfrac{B_1}{2A_1},F_{b,\min}<-\dfrac{B_2}{2A_2}<F_{b,\max},\\F_{b,\max},F_{b,\max}<-\dfrac{B_2}{2A_2}.\end{cases}\end{cases}\tag{26}$$

Therefore, optimization problem (20) is transformed into an indirect optimization problem for determining the initial values of $\lambda(s_0)$, as shown in Figure 5.

The form of the corresponding indirect optimization problem is

$$\min_{\lambda(s_0)\in R}J_\lambda\left(\lambda\left(s_0\right)\right)=\left\|\lambda\left(s_f\right)-2\phi_L\left(v_x\left(s_f\right)-v_{x,\mathrm{ref}}\left(s_f\right)\right)\right\|.\tag{27}$$

At the initial position, vehicle speed $v_x(s_0)$ is obtained by sensors, and the initial value of the covariate variable $\lambda(s_0)$ is given. According to (25) and (26), the control inputs $F_t(s_0)$ and $F_b(s_0)$ can be obtained.

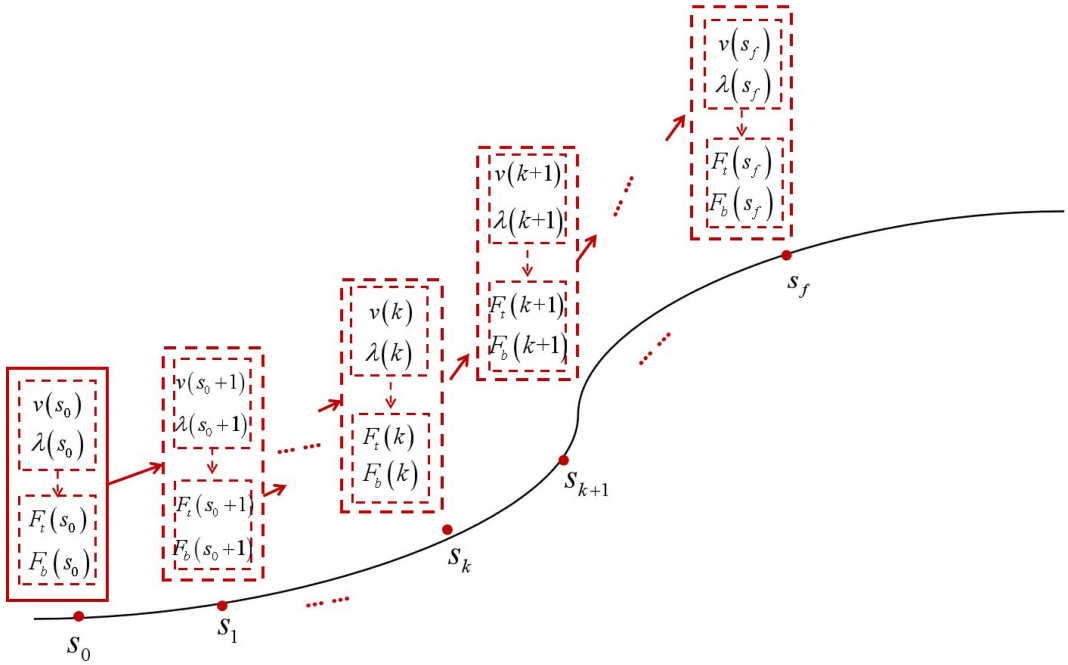

Figure 5 (Color online) Iterative solution for indirect optimization problems.

Combined with (16) and (22), we can get $v(s_0+1)$ and $\lambda(s_0+1)$ for the next position. In this way, the $v_x(s_f)$ and $\lambda(s_0)$ for the terminal position can be recursively obtained. Therefore, the relationship between the initial position $v_x(s_0)$ and $\lambda(s_0)$ corresponding to the terminal position $v_x(s_f)$ and $\lambda(s_0)$ is established. By solving the optimization problem (27), the control variables can be obtained.

To quickly solve the indirect optimization problem (27), this article uses the dichotomy method. To ensure that the dichotomy method can obtain the solution of (27), $\lambda(s_0)$ must be monotonic, and the signs of $J_\lambda(\lambda(\Lambda_L))$ and $J_\lambda(\lambda(\Lambda_U))$ need to be different within the feasible set $\lambda(s_0) \in [\Lambda_L, \Lambda_U]$. The proof of the monotonicity of $\lambda(s_0)$ within the feasible set $\lambda(s_0) \in [\Lambda_L, \Lambda_U]$ is shown in Appendix A, and the proof that the signs of $J_\lambda(\lambda(\Lambda_L))$ and $J_\lambda(\lambda(\Lambda_U))$ are different is shown in Appendix B.

To further explain the influence of parameters in the optimization problem, a combination of parameters that partially satisfy the theorem conditions is selected, and the curves of the solutions of the indirect optimization problem and the original optimization problem are plotted, as shown in Figure 6. It can be seen that after satisfying the theorem, the values of both the indirect optimization problem and the original optimization problem will change. However, the indirect optimization problem will have a unique global optimal solution, while the original optimization problem will correspondingly have an optimal solution.

The existence of a solution and the convergence of the solution process are shown in Figure 7. The binary method can converge to the optimal solution after approximately 5 iterations.

To verify the effectiveness of the algorithm on actual vehicles, we conducted a longitudinal speed control algorithm validation on a four-wheel drive vehicle, using the driver's driving speed as the reference vehicle speed and the experimental results are shown in Figure 8. It can be seen that excluding some burrs caused by sensor noise, the longitudinal control algorithm proposed in this section can effectively control the vehicle speed to follow the referenced speed in terms of accuracy and trend.

3.2 Design of a lateral vehicle controller based on back-stepping

To track the planned heading angle, a deviation model is established. The specific form of the lateral deviation model is

$$\dot{e}_d(s) = v_x(s) e_\varphi(s), \tag{28}$$

$$\dot{e}_\varphi(s) = \frac{v_r(s)}{L}\delta_f(s) - \kappa(s) v_x(s), \tag{29}$$

where e_d is the lateral error of the vehicle compared to the reference trajectory, $e_\varphi(s)$ is the heading angle error of the vehicle compared to the reference trajectory, v_r is the vehicle's tot velocity, v_x is the vehicle's

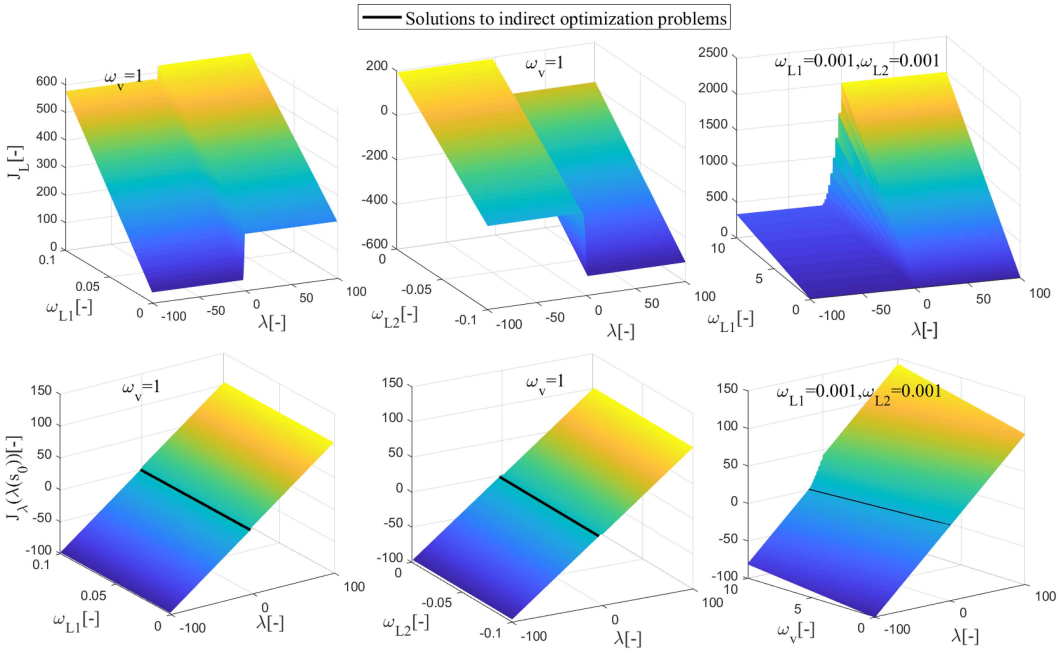

Figure 6 (Color online) Optimal solutions of the direct and indirect optimization problems under different parameters.

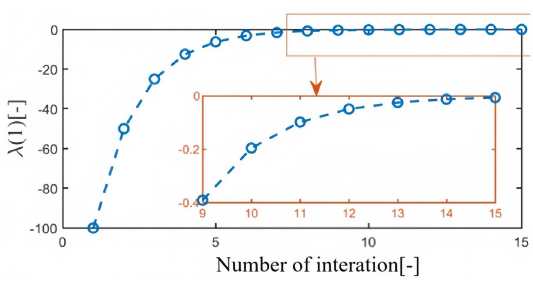

Figure 7 (Color online) Proof of convergence for solving indirect optimization problems.

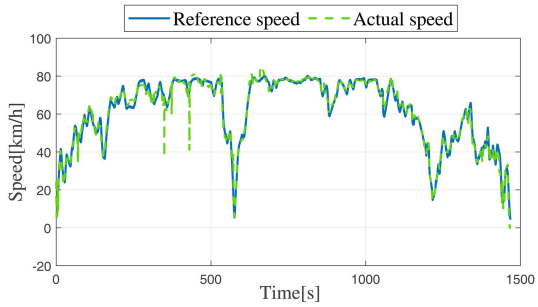

Figure 8 (Color online) Speed control results of actual vehicle experiments.

longitudinal velocity, L is the vehicle's wheelbase, κ is the road curvature and δ_f is the steering wheel angle calculated by the controller.

Because the deviation systems (28) and (29) are cascaded systems, deriving the e_φ^* that can make the e_d tend to zero, the tracking error is set as

$$e_1(s) = e_d(s) - 0 = e_d(s). \tag{30}$$

We set the Lyapunov function as

$$V_1 = \frac{1}{2} e_1(s)^2. \tag{31}$$

Then, taking the derivative of (31), we have

$$\dot{V}_1 = e_1(s)\dot{e}_1(s) = e_1(s)\dot{e}_d(s) = e_1(s)v_x(s)e_\varphi(s). \tag{32}$$

Introduce the controller parameter K_1 that causes the e_d tends to zero, we set

$$e_1(s)v_x(s)e_\varphi(s) = -K_1 e_1(s)^2. \tag{33}$$

Then, we have

$$\dot{V}_1 = -K_1 e_1(s)^2 \leqslant 0. \tag{34}$$

Therefore, the virtual control input e_φ^* that can make e_d towards zero is

$$e_\varphi(s)^* = -\frac{K_1}{v_x(s)} e_1(s). \tag{35}$$

The virtual tracking error between e_φ and e_φ^* is defined as

$$e_2(s) = e_\varphi(s) - e_\varphi(s)^*. \tag{36}$$

We set Lyapunov function $V_2 = \frac{1}{2}e_1(s)^2 + \frac{1}{2}e_2(s)^2$ and take the derivative of V_2:

$$\begin{aligned}
\dot{V}_2 &= e_1(s)\dot{e}_1(s) + e_2(s)\dot{e}_2(s) \\
&= e_1(s)v_x(s)e_\varphi(s) + e_2(s)\dot{e}_2(s) \\
&= e_1(s)v_x(s)\left[e_2(s) + e_\varphi(s)^*\right] + e_2(s)\dot{e}_2(s) \\
&= e_1(s)v_x(s)e_\varphi(s)^* + e_2(s)\left[e_1(s)v_x(s) + \dot{e}_2(s)\right] \\
&= -K_1 e_1(s)^2 + e_2(s)\left[e_1(s)v_x(s) + \dot{e}_2(s)\right] \\
&= -K_1 e_1(s)^2 + e_2(s)\left[e_1(s)v_x(s) + \dot{e}_\varphi(s) - \dot{e}_\varphi(s)^*\right] \\
&= -K_1 e_1(s)^2 + e_2(s)\left[\frac{v_r(s)}{L}\delta_f - \kappa v_x(s) - \dot{e}_\varphi(s)^* + e_1(s)v_x(s)\right].
\end{aligned} \tag{37}$$

Introduce the controller parameter K_2 that makes $e_\varphi = e_\varphi^*$:

$$\left[\frac{v_r(s)}{L}\delta_f - \kappa v_x(s) - \dot{e}_\varphi(s)^* + e_1(s)v_x(s)\right] = -K_2 e_2(s). \tag{38}$$

Then, we have

$$\dot{V}_2 = -K_1 e_1(s)^2 - K_2 e_2(s)^2 \leqslant 0. \tag{39}$$

Therefore, by combining (38), the optimal steering wheel angle is

$$\delta_f = \frac{L}{v_r(s)}\left[-K_2 e_\varphi(s) + \kappa v_x(s) - K_1 e_\varphi(s) - e_d(s)v_x(s)\right]. \tag{40}$$

Because the solution of the back-stepping controller does not involve optimization calculations, according to (28) and (29), the adjustment of heading error can indirectly affect the lateral error, and according to (40), the influence of control parameters on the lateral and heading errors is the same. Therefore, in subsequent simulation and actual vehicle experiments, K_1 and K_2 are on the same order of magnitude, and we set $K_2 \geqslant K_1$.

To verify the effectiveness of the designed lateral control algorithm, we conducted experiments on a four-wheel drive vehicle. Designed a lateral trajectory containing sine, slope, and fixed values as reference values. The results are shown in Figure 9. It can be seen that, after excluding sensor noise, the controller can effectively control the vehicle to track the required lateral position.

This section discusses longitudinal and lateral decoupling control of the vehicle in the Frenet coordinate system. According to the lateral error equations (28) and (29), the tracking error of the vehicle's longitudinal speed will impact the effectiveness of the lateral controller. Therefore, it is necessary to analyze the robustness of the back-stepping controller under the influence of longitudinal speed tracking error. Please refer to Appendix C for the specific proof.

4 Simulation and analysis

4.1 Comparison experiment with existing methods

To compare the effectiveness of the proposed controller in this article with existing methods, we compare the control effect with commonly used PI controllers in the automotive industry. The results of the PMP controller and PI controller are shown in Figure 10. It can be seen that both the PMP controller and the PI controller can maintain a good tracking control effect on the slope signal. However, when the

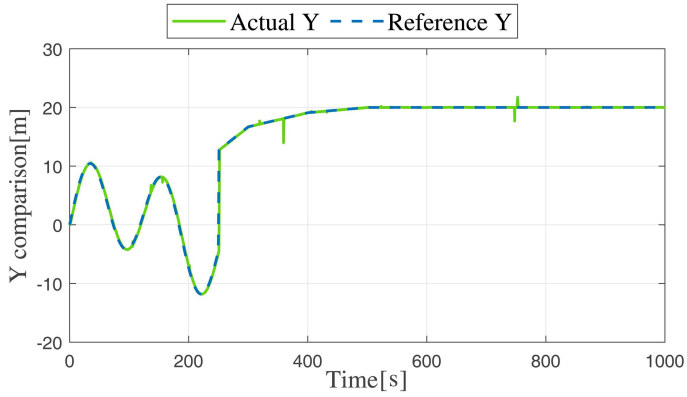

Figure 9 (Color online) Lateral control results of actual vehicle experiments.

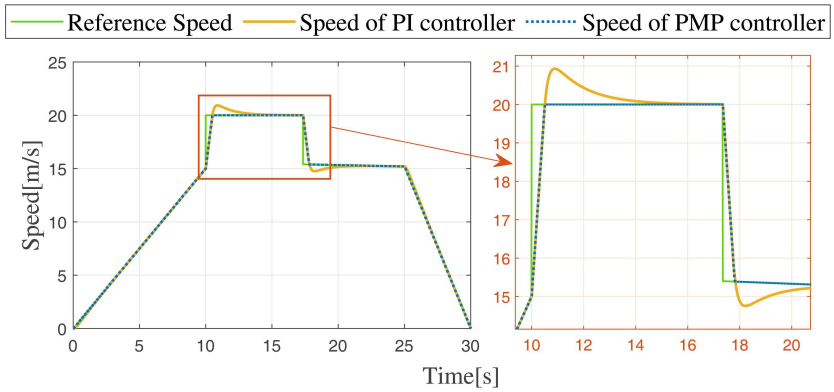

Figure 10 (Color online) Comparison of PI controller and the proposed controller in longitudinal vehicle speed tracking.

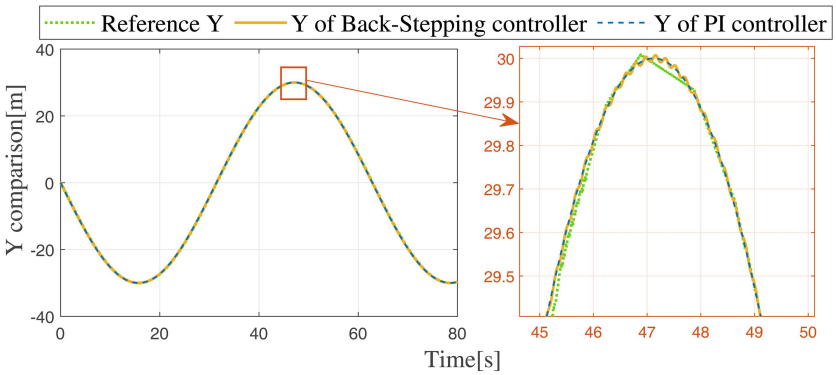

Figure 11 (Color online) Comparison of PI controller and the proposed controller in lateral control.

speed step occurs, the PI controller will bring a partial overshoot. Moreover, when the parameters are suitable, the PMP controller can reduce overshoot by sacrificing some response speed. This is important for vehicles with weak robustness when experiencing a tire blowout

Comparing the control effect of the back-stepping controller and PI controller by using a sinusoidal reference signal. It can be seen from Figure 11 that the adjustment frequency of the back-stepping controller is smaller than that of the PI controller. This means the vehicle's yaw angle more smoother, reducing interference on the stable operation of the vehicle with a tire blowout.

Because the back-stepping controller does not involve iterative calculation, its calculation time is not significantly different from the PI controller. This article only focuses on the calculation time of the PMP controller. To verify whether the calculation time of the proposed method can meet the requirements of the hardware in practical applications, the overall computing time during operation is shown in Figure 12, as well as the computing times of the PI controller and the proposed controller at

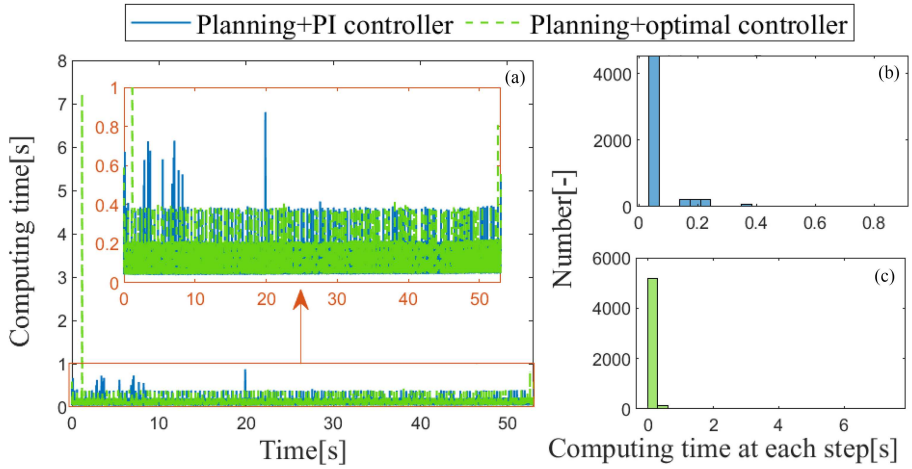

Figure 12 (Color online) Comparison and statistical analysis of single step calculation time between the proposed method and PI control method. (a) Computing time at each step; (b) planning+PI controller; (c) planning+optimal controller.

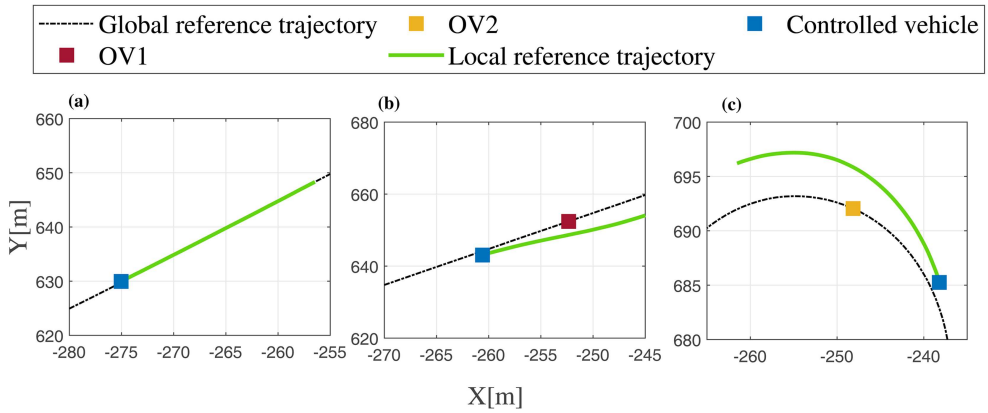

Figure 13 (Color online) Offline simulation of obstacle avoidance planning. (a) Tracking reference trajectory; (b) avoiding obstacles on straight road; (c) avoiding obstacles on curve.

each step. The computing times in most cases using the proposed method are less than 50 ms. By comparing the calculation times, it can be seen that the longitudinal PMP controller has little impact on the single-step computing time. Moreover, from the overall-time statistical analysis and comparison, it can be seen that compared with PI controllers commonly used in industry, the method proposed in this article has a 5.7% longer computing time. However, the shorter single-step computing time indicates smoother vehicle operation, which is crucial for vehicles with tire blowout.

Simulation testing can help quickly validate an algorithm during the development stage of autonomous driving or assisted driving. Compared to tests with actual vehicles, it is safer, more efficient, more cost-effective, and easier to replicate. Therefore, the control structure and algorithm proposed in this article are simulated and verified by Carsim and Simulink co-simulation with a dataset collected for an actual road, and the simulation results are analyzed.

When OV operation does not affect EV operation, the EV needs to track the global reference trajectory, as shown in the subgraph of the tracking reference path in Figure 13. Under this control framework, the vehicle tracking reference trajectory can be well controlled. When obstacles appear in front of the vehicle's trajectory and affect EV operation, the proposed method can plan reasonable obstacle avoidance trajectories for both straight and curved roads.

To verify the effectiveness of the proposed method in a dynamic traffic flow, we plan the obstacle avoidance trajectories and control the Carsim vehicle model to track the trajectories, as shown in Figure 14. In a dynamic traffic flow, the proposed decision and planning methods can provide reasonable local obstacle avoidance trajectories with a larger obstacle avoidance radius, and the overall trajectory curvature is smoother, ensuring overall tracking of the initial global reference trajectory while avoiding moving OVs.

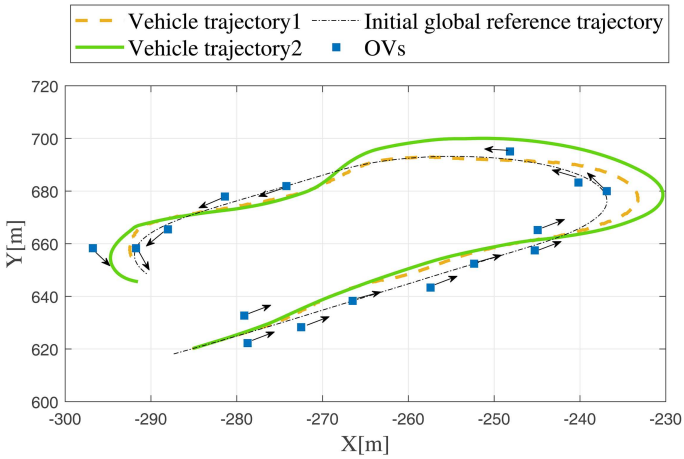

Figure 14 (Color online) Real time obstacle avoidance planning simulation in traffic flow.

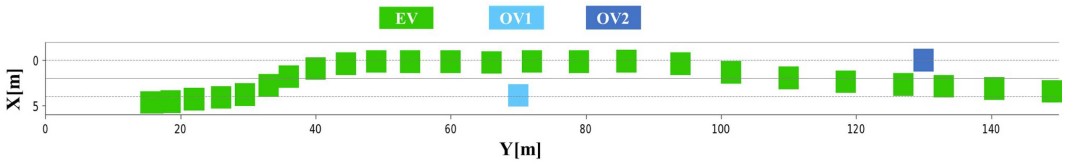

Figure 15 (Color online) Static obstacle vehicle test.

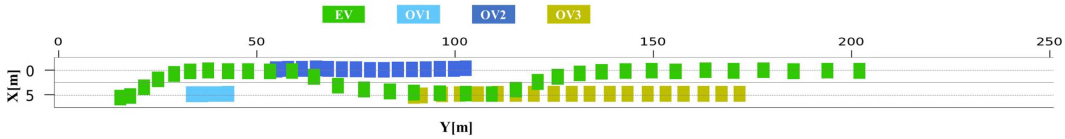

Figure 16 (Color online) Dynamic obstacle vehicle test.

4.2 Real vehicle obstacle avoidance experiment

After the above simulation experiments and comparative analysis, we have proven the effectiveness of the planning and control method designed in this paper for the safe and stable operation of tire blowout vehicle. We conduct overall planning and control experiments based on a four-wheel drive vehicle. The experiments are divided into two parts, namely obstacle avoidance operation on static obstacles and obstacle avoidance operation on dynamic obstacles. Due to safety and site limitations, we conducted these two experiments on a straight road within 300 m.

Conducting the first experiment with two static obstacle vehicles, which is shown in Figure 15. It can be seen that the proposed planning method, which considers the kinematic limitations of tire blowout vehicles can smoothly plan the obstacle avoidance trajectory at a distance of more than 50 m from the obstacles, and also can achieve accurate and stable control of the vehicle.

Conducting the second experiment with dynamic obstacle vehicles, shown in Figure 16. The overlap between the EV and the OVs in the figure indicates that the current position of the EV overlaps with the historical position of the OVs, and does not represent a collision between the vehicles. It can be seen that in the moving traffic flow, the proposed method can plan and control the EV to smoothly avoid obstacles, ensuring the safe and stable operation of the vehicle with a tire blowout in the traffic flow.

Figures 17 and 18 are live shots from the actual vehicle experiment, the two images depict the vehicle avoiding two dynamic obstacles consecutively after a tire blowout, captured from the side and rear perspectives. The results indicate that the proposed planning and control algorithm effectively plans obstacle avoidance trajectories and achieves good control in real-time operation.

Figure 19 is an enlarged view of the controlled vehicle avoiding the second obstacle, showing a zero-pressure tire (red box) simulating a tire after the blowout, alongside an intact tire (green box). This demonstrates our planning method's ability to consider tire blowout kinematic constraints and devise feasible obstacle avoidance trajectories.

Figure 17 (Color online) Real-vehicle experiment: live shots 1.

Figure 18 (Color online) Real-vehicle experiment: live shots 2.

Figure 19 (Color online) Locally enlarged view of the real-vehicle experiment.

5 Conclusion

This article presents a trajectory planning and control method for vehicles with tire blowouts in traffic flows. The vehicle state and road parameters are transformed from the Cartesian coordinate system into the Frenet coordinate system by decoupling lateral and longitudinal vehicle motion. First, the criteria for the available paths for obstacle avoidance are obtained through the structured representation of roads. Second, according to the constraints of vehicle dynamics, the feasible states of the vehicle are gridded, and real-time obstacle avoidance of the vehicle while driving stably to a safe place in a complex traffic flow is planned. Third, during longitudinal vehicle control in the long-distance domain, to reduce driver tension, save vehicle energy and ensure comfort and low energy consumption, the longitudinal speed model predictive tracking optimization problem is constructed, and this problem is quickly solved by incorporating the PMP; the existence of the optimal solution is proved. Then, to ensure rapid and safe lateral obstacle avoidance by the vehicle in the short-time domain, and to ensure the stability of the vehicle during lateral obstacle avoidance under longitudinal speed tracking errors, a lateral vehicle controller is designed based on back-stepping, and it is proved that this controller can ensure the Lyapunov stability of the vehicle under longitudinal tracking errors. Finally, the effectiveness of the proposed planning-domain control method is verified and analyzed through simulation.

Acknowledgements This work was supported by Research on the Quasi-Mechanical Load Response Mechanism and Safety Reliability of Autonomous Vehicles (Grant No. 52172388).

References

1 Huang J, Guo K, Song X, et al. Vehicle stability control method after tire blowout. China Mech Eng, 2009, 20: 2006–2010

2 Wang F, Chen H, Guo K, et al. A novel integrated approach for path following and directional stability control of road vehicles after a tire blow-out. Mech Syst Signal Process, 2017, 93: 431–444
3 Wang F, Chen H, Cao D. Nonlinear coordinated motion control of road vehicles after a tire blowout. IEEE Trans Contr Syst Technol, 2015, 24: 956–970
4 Wang F, Chen H, Guo L L, et al. Predictive safety control for road vehicles after a tire blowout. Sci China Inf Sci, 2018, 61: 070209
5 Liu K, Gong J, Kurt A, et al. Dynamic modeling and control of high-speed automated vehicles for lane change maneuver. IEEE Trans Intell Veh, 2018, 3: 329–339
6 Huang Y, Wang H, Khajepour A, et al. A novel local motion planning framework for autonomous vehicles based on resistance network and model predictive control. IEEE Trans Veh Technol, 2020, 69: 55–66
7 Bevly D, Cao X, Gordon M, et al. Lane change and merge maneuvers for connected and automated vehicles: a survey. IEEE Trans Intell Veh, 2016, 1: 105–120
8 Gonzalez D, Perez J, Milanes V, et al. A review of motion planning techniques for automated vehicles. IEEE Trans Intell Transp Syst, 2016, 17: 1135–1145
9 Yu Z, Li Y, Xiong L. A review of the motion planning problem of automous vehicle. J Tongji Univ (Nat Sci), 2017, 45: 1150–1159
10 Xing S, Chen X, He W, et al. An autonomous obstacle avoidance method based on artificial potential field and improved A* algorithm for UAV. ITM Web Conf, 2022, 47: 02016
11 Tang B, Hirota K, Wu X, et al. Path planning based on improved hybrid A* algorithm. J Adv Comput Intell Intell Inform, 2021, 25: 64–72
12 Li M, Fu J, Zhang Y, et al. The improved algorithm based on DFS and BFS for indoor trajectory reconstruction. In: Proceedings of International Conference on Wireless Algorithms, Systems, and Applications, 2016. 464–474
13 Liu H W, Luo W B. The study on DFS algorithm of unmanned aerial vehicle platform communications relay system. Appl Mech Mater, 2014, 721: 662–665
14 Baswana S, Khan S. Incremental algorithm for maintaining a DFS tree for undirected graphs. Algorithmica, 2017, 79: 466–483
15 Tahlyan D, Pinjari A R. Performance evaluation of choice set generation algorithms for analyzing truck route choice: insights from spatial aggregation for the breadth first search link elimination (BFS-LE) algorithm. Transpmetrica A-Transp Sci, 2020, 16: 1030–1061
16 Tan W, Hu Y, Zhao Y, et al. Heterogeneous multi UAV mission planning based on ant colony algorithm powered BP neural network. Comput Intell Neurosci, 2021, 2021: 4369201
17 Jiang L, Wang J, Liang C, et al. Research on crowdsourcing distribution path based on improved ant colony algorithm (in Chinese). Comput Eng Appl, 2019, 55: 244–249
18 He B, Jaemin L, Ufuk T, et al. BP-RRT: barrier pair synthesis for temporal logic motion planning. In: Proceedings of the 59th IEEE Conference on Decision and Control, Jeju Island, 2020. 14–18
19 Zheng H. Research on cooperative production planning method based on factor analysis and BP neural network model. In: Smart Innovation, Systems and Technologies. Berlin: Springer, 2021. 85–93
20 Lathrop P, Boardman B, Martinez S. Distributionally safe path planning: Wasserstein safe RRT. IEEE Robot Autom Lett, 2022, 7: 430–437
21 Chai Q, Wang Y. RJ-RRT: improved RRT for path planning in narrow passages. Appl Sci, 2022, 12: 12033
22 Xu W, Yang Y, Yu L, et al. A global path planning algorithm based on improved RRT (in Chinese). Control Dec, 2022, 37: 829–838
23 Li J, Chen Y, Zhao X N, et al. An improved DQN path planning algorithm. J Supercomput, 2022, 78: 616–639
24 Chen L, Hu X, Tang B, et al. Conditional DQN-based motion planning with fuzzy logic for autonomous driving. IEEE Trans Intell Transp Syst, 2022, 23: 2966–2977
25 Khan A, Zhang J, Ahmad S, et al. DQN-based proactive trajectory planning of UAVs in multi-access edge computing. Comput Mater Continua, 2023, 74: 4685–4702
26 Zhou Y, Yuan C, Xie H, et al. Collision avoidance path planning of tourist ship based on DDPG algorithm. Chinese J Ship Res, 2021, 16: 19–26
27 Zhou S, Shan L, Chang L, et al. Robot path planning algorithm based on improved DDPG algorithm (in Chinese). J Nanjing Univ Sci Technol, 2021, 45: 265–270
28 Chu D, Li H, Zhao C, et al. Trajectory tracking of autonomous vehicle based on model predictive control with PID feedback. IEEE Trans Intell Transp Syst, 2023, 24: 2239–2250
29 Manuel C J T, Santos M M D, Lenzi G G, et al. Computational validation of the best tuning method for a vehicle-integrated PID controller. Model Simul Eng, 2022, 2022: 1–16
30 Guo R, Ding Y, Yue X. Active adaptive continuous nonsingular terminal sliding mode controller for hypersonic vehicle. Aerospace Sci Tech, 2023, 137: 108279
31 Ma Y, Zhao J Y, Zhao H Y, et al. Longitudinal-vertical integrated sliding mode controller for distributed electric vehicles. Sci China Inf Sci, 2020, 63: 219201
32 Ge Z, Man Z, Wang Z, et al. Robust adaptive sliding mode control for path tracking of unmanned agricultural vehicles. Comput Electrical Eng, 2023, 108: 108693
33 Cai G, Xu L, Liu Y, et al. Robust preview path tracking control of autonomous vehicles under time-varying system delays and saturation. IEEE Trans Veh Technol, 2023, 72: 8486–8499
34 Guan H, He F, Cui W F, et al. Research on the unified preview decision model for the longitudinal control of the intelligent vehicle. Proc Inst Mech Eng Part D-J Autom Eng, 2022, 236: 1259–1274
35 Mattas K, Botzoris G, Papadopoulos B. Safety aware fuzzy longitudinal controller for automated vehicles. J Traffic Transp Eng (Engl Ed), 2021, 8: 568–581
36 Chu H Q, Guo L L, Yan Y J, et al. Energy-efficient longitudinal driving strategy for intelligent vehicles on urban roads. Sci China Inf Sci, 2019, 62: 064201
37 Li Z H, Wang P, Zhu C J, et al. MPC-based strategy for longitudinal and lateral stabilization of a vehicle under extreme conditions. Sci China Inf Sci, 2022, 65: 179203
38 Zheng X, Li H, Ahn C K, et al. NN-based fixed-time attitude tracking control for multiple unmanned aerial vehicles with nonlinear faults. IEEE Trans Aerosp Electron Syst, 2023, 59: 1738–1748
39 Liu Y, Yao D, Li H, et al. Distributed cooperative compound tracking control for a platoon of vehicles with adaptive NN. IEEE Trans Cybern, 2022, 52: 7039–7048
40 Shinde S S, Tarchi D. Collaborative reinforcement learning for multi-service internet of vehicles. IEEE Int Things J, 2023, 10: 2589–2602
41 Wang Q, Ju F, Zhuang W C, et al. Ecological cruising control of connected electric vehicle: a deep reinforcement learning approach. Sci China Tech Sci, 2022, 65: 529–540
42 Yu H, Tseng H E, Langari R. A human-like game theory-based controller for automatic lane changing. Transp Res Part C-Emerg Technol, 2018, 88: 140–158

43 Czubenko M, Kowalczuk Z, Ordys A. Autonomous driver based on an intelligent system of decision-making. Cogn Comput, 2015, 7: 569–581
44 Hou Y, Edara P, Sun C. Situation assessment and decision making for lane change assistance using ensemble learning methods. Expert Syst Appl, 2015, 42: 3875–3882
45 Yang L. Research on automated hazard escaping control method for distributed drive vehicles after a tire blowout. Dissertation for Ph.D. Degree. Dalian: Dalian University of Technology, 2020
46 Yang B, Song X, Gao Z. Optimal obstacle avoidance trajectory planning algorithm considering (in Chinese). Autom Eng, 2021, 43: 562–570

Appendix A $J_{\lambda}(\lambda(s_0))$ monotonicity proof

When implementing the algorithm in hardware, the iterations of the state variables and covariates are both progressive in the time domain. Considering (15), with a discrete time interval of dt and the current time $t=k$, the following situations are discussed: a continuous vehicle acceleration operation or constant speed operation, a continuous vehicle deceleration operation, an acceleration-to-deceleration vehicle operation, and a deceleration-to-acceleration vehicle operation.

Appendix A.1 Continuous vehicle acceleration operation

If the vehicle performs continuous acceleration, the abscissa of the extreme point of the quadratic function in (26) is

$$-\frac{B_1(k)}{2A_1(k)}=-\frac{\lambda(k)}{\omega_{L1}Mrv_x(k)^2}. \tag{A1}$$

We select two covariate variables $\lambda_1(k)$ and $\lambda_2(k)$ with corresponding control quantities $F_{t,1}(k)$ and $F_{t,2}(k)$, then use time $k=1$ as the starting time of the prediction time domain, given $\lambda_1(1)>\lambda_2(1)$. Then, we recursively extrapolate to $\lambda_1(t_f)$ and $\lambda_2(t_f)$. Because $v_{x,1}(1)=v_{x,2}(1)=v_{x,0}$ at the starting time, the corresponding optimal control quantity for $\lambda_1(1)$ and $\lambda_2(1)$ is

$$F_{t,1}(1)=-\frac{\lambda_1(1)}{\omega_{L1}Mrv_{x,1}(1)^2}<F_{t,2}(1)=-\frac{\lambda_2(1)}{\omega_{L1}Mrv_{x,2}(1)^2}. \tag{A2}$$

According to (16), we have

$$\dot{v}_{x,1}(1)=\frac{F_{t,1}(1)}{Mr}-C_rg\cos(\theta)<\dot{v}_{x,2}(1)=\frac{F_{t,2}(1)}{Mr}-C_rg\cos(\theta). \tag{A3}$$

Therefore, the following relationship holds at time $k=2$:

$$v_{x,1}(2)<v_{x,2}(2). \tag{A4}$$

According to (22), the following relationship holds between $\dot{\lambda}_1(1)$ and $\dot{\lambda}_2(1)$ at $k=1$:

$$\dot{\lambda}_1(1)=-[2\omega_{L1}F_{t,1}(1)^2v_{x,1}(1)+2\omega_{L3}(v_{x,1}(1)-v_{x,\mathrm{ref}}(1))]>\dot{\lambda}_2(1)=-[2\omega_{L1}F_{t,2}(1)^2v_{x,2}(1)+2\omega_{L3}(v_{x,2}(1)-v_{x,\mathrm{ref}}(1))]. \tag{A5}$$

Then, we have the following relationship between $\lambda_1(2)$ and $\lambda_2(2)$ at time $k=2$:

$$\lambda_1(2)=\lambda_1(1)+\dot{\lambda}_1(1)\mathrm{d}t>\lambda_2(2)=\lambda_2(1)+\dot{\lambda}_2(1)\mathrm{d}t. \tag{A6}$$

Therefore, at time $k=2$, we have

$$F_{t,1}(2)=-\frac{\lambda_1(2)}{\omega_{L1}Mrv_{x,1}(2)^2}<F_{t,2}(2)=-\frac{\lambda_2(2)}{\omega_{L1}Mrv_{x,2}(2)^2}. \tag{A7}$$

It can be recursively inferred that

$$\dot{v}_{x,1}(2)=-\frac{F_{b,1}(2)}{Mr}-C_rg\cos(\theta)<\dot{v}_{x,2}(2)=-\frac{F_{b,2}(2)}{Mr}-C_rg\cos(\theta). \tag{A8}$$

Here, Eq. (A8) is consistent with (A3). Then, the remaining recursive process until the terminal time is consistent with (A4)–(A7). At the terminal time of the prediction horizon, it can be obtained that

$$\lambda_1(t_f)>\lambda_2(t_f),v_{x,1}(t_f)<v_{x,2}(t_f). \tag{A9}$$

Therefore, it can be obtained that

$$J_{\lambda,1}(\lambda_1(1))=\lambda_1(t_f)-2\phi_L\left(v_{x,1}(t_f)-v_{x,\mathrm{ref}}(t_f)\right)>J_{\lambda,2}(\lambda_2(1))=\lambda_2(t_f)-2\phi_L\left(v_{x,2}(t_f)-v_{x,\mathrm{ref}}(t_f)\right). \tag{A10}$$

As the vehicle continues to accelerate, $J_{\lambda}(\lambda_1(1))$ monotonically increases as $\lambda(1)$ increases.

Appendix A.2 Continuous vehicle deceleration operation

If the vehicle performs continuous deceleration, the abscissa of the extreme point of the quadratic function in (26) is

$$-\frac{B_2(k)}{2A_2(k)}=\frac{\lambda(k)}{\omega_{L2}Mr}. \tag{A11}$$

We select two covariate variables $\lambda_1(k)$ and $\lambda_2(k)$ with corresponding control variables $F_{b,1}(k)$ and $F_{b,2}(k)$ and take this time as the start of the prediction time horizon $k=1$. Given $\lambda_1(1)>\lambda_2(1)$, we iterate to $\lambda_1(t_f)$ and $\lambda_2(t_f)$. Because $v_{x,1}(1)=v_{x,2}(1)=v_{x,0}$ holds at the start time, the optimal control quantities for $\lambda_1(1)$ and $\lambda_2(1)$ are

$$F_{b,1}(1)=\frac{\lambda_1(1)}{\omega_{L2}Mr}>F_{b,2}(1)=\frac{\lambda_2(1)}{\omega_{L2}Mr}. \tag{A12}$$

According to (16),

$$\dot{v}_{x,1}(1)=-\frac{F_{b,1}(1)}{Mr}-C_rg\cos(\theta)<\dot{v}_{x,2}(1)=-\frac{F_{b,2}(1)}{Mr}-C_rg\cos(\theta). \tag{A13}$$

Therefore, at time $k=2$, the following relationship holds:

$$v_{x,1}(2)<v_{x,2}(2). \tag{A14}$$

According to (22), at time $k=1$, the following relationship holds between $\dot{\lambda}_1(1)$ and $\dot{\lambda}_2(1)$:

$$\dot{\lambda}_1(1)=-[2\omega_{L1}F_{t,1}(1)^2v_{x,1}(1)+2\omega_{L3}(v_{x,1}(1)-v_{x,\mathrm{ref}}(1))]>\dot{\lambda}_2(1)=-[2\omega_{L1}F_{t,2}(1)^2v_{x,2}(1)+2\omega_{L3}(v_{x,2}(1)-v_{x,\mathrm{ref}}(1))]. \tag{A15}$$

Then, at time $k=2$, the following relationship holds between $\lambda_1(2)$ and $\lambda_2(2)$:

$$\lambda_1(2)=\lambda_1(1)+\dot{\lambda}_1(1)\mathrm{d}t>\lambda_2(2)=\lambda_2(1)+\dot{\lambda}_2(1)\mathrm{d}t. \tag{A16}$$

Therefore, at time $k=2$, we have

$$F_{b,1}(2)=\frac{\lambda_1(2)}{\omega_{L2}Mr}>F_{b,2}(2)=\frac{\lambda_2(2)}{\omega_{L2}Mr}. \tag{A17}$$

Then, we recursively obtain

$$\dot{v}_{x,1}(2)=-\frac{F_{b,1}(2)}{Mr}-C_rg\cos(\theta)<\dot{v}_{x,2}(2)=-\frac{F_{b,2}(2)}{Mr}-C_rg\cos(\theta). \tag{A18}$$

If the relationship between (A18) and (A13) is consistent, then the remaining recursive process until the terminal time is consistent with (A14)–(A17). When predicting the terminal time, it can be obtained that

$$\lambda_1(t_f)>\lambda_2(t_f),v_{x,1}(t_f)<v_{x,2}(t_f). \tag{A19}$$

Therefore, it can be obtained that

$$J_{\lambda,1}\left(\lambda_1(1)\right)=\lambda_1(t_f)-2\phi_L\left(v_{x,1}(t_f)-v_{x,\mathrm{ref}}(t_f)\right)>J_{\lambda,2}\left(\lambda_2(1)\right)=\lambda_2(t_f)-2\phi_L\left(v_{x,2}(t_f)-v_{x,\mathrm{ref}}(t_f)\right). \tag{A20}$$

Therefore, as the vehicle continues to slow down, $J_\lambda\left(\lambda_1(1)\right)$ monotonically increases as $\lambda(1)$ increases.

Appendix A.3 Acceleration-to-deceleration operation

If the vehicle is accelerating or maintaining a constant speed at the current moment, the horizontal coordinate value of the extreme point of the quadratic function in (26) is

$$-\frac{B_2(k)}{2A_2(k)}=\frac{\lambda(k)}{\omega_{L2}Mr}. \tag{A21}$$

We select two covariate variables $\lambda_1(k)$ and $\lambda_2(k)$ with corresponding control inputs of $F_{b,1}(k)$ and $F_{b,2}(k)$ and take the current time $k=1$ as the starting time of the prediction horizon. Given $\lambda_1(1)>\lambda_2(1)$, we recursively extrapolate to $\lambda_1(t_f)$ and $\lambda_2(t_f)$. At the starting time, $v_{x,1}(1)=v_{x,2}(1)=v_{x,0}$, so the corresponding optimal control inputs for $\lambda_1(1)$ and $\lambda_2(1)$ are

$$F_{b,1}(1)=\frac{\lambda_1(1)}{\omega_{L2}Mr}>F_{b,2}(1)=\frac{\lambda_2(1)}{\omega_{L2}Mr}. \tag{A22}$$

According to (16), we have

$$\dot{v}_{x,1}(1)=-\frac{F_{b,1}(1)}{Mr}-C_rg\cos(\theta)<\dot{v}_{x,2}(1)=-\frac{F_{b,2}(1)}{Mr}-C_rg\cos(\theta). \tag{A23}$$

Therefore, at time $k=2$, the following relationship holds:

$$v_{x,1}(2) < v_{x,2}(2). \tag{A24}$$

According to (22), at time $k=1$, the following relationship holds:

$$\dot{\lambda}_1(1) = -[2\omega_{L1}F_{t,1}(1)^2 v_{x,1}(1) + 2\omega_{L3}(v_{x,1}(1) - v_{x,\mathrm{ref}}(1))] > \dot{\lambda}_2(1) = -[2\omega_{L1}F_{t,2}(1)^2 v_{x,2}(1) + 2\omega_{L3}(v_{x,2}(1) - v_{x,\mathrm{ref}}(1))]. \tag{A25}$$

Then, at time $k=2$, the following relationship holds:

$$\lambda_1(2) = \lambda_1(1) + \dot{\lambda}_1(1)\mathrm{d}t > \lambda_2(2) = \lambda_2(1) + \dot{\lambda}_2(1)\mathrm{d}t. \tag{A26}$$

When the vehicle decelerates at the next time $k=2$, we have

$$F_{b,1}(2) = \frac{\lambda_1(2)}{\omega_{L2}Mr} > F_{b,2}(2) = \frac{\lambda_2(2)}{\omega_{L2}Mr}. \tag{A27}$$

Then, we recursively obtain

$$\dot{v}_{x,1}(2) = -\frac{F_{b,1}(2)}{Mr} - C_r g\cos(\theta) < \dot{v}_{x,2}(2) = -\frac{F_{b,2}(2)}{Mr} - C_r g\cos(\theta). \tag{A28}$$

If the relationship between (A28) and (A23) is consistent, then the remaining recursive process until the terminal time is consistent with (A24)–(A27). At the terminal time, it can be obtained that

$$\lambda_1(t_f) > \lambda_2(t_f), \quad v_{x,1}(t_f) < v_{x,2}(t_f). \tag{A29}$$

Therefore, it can be obtained that

$$J_{\lambda,1}\left(\lambda_1(1)\right) = \lambda_1(t_f) - 2\phi_L\left(v_{x,1}(t_f) - v_{x,\mathrm{ref}}(t_f)\right) > J_{\lambda,2}\left(\lambda_2(1)\right) = \lambda_2(t_f) - 2\phi_L\left(v_{x,2}(t_f) - v_{x,\mathrm{ref}}(t_f)\right). \tag{A30}$$

As the vehicle changes from accelerating to decelerating, $J_\lambda\left(\lambda_1(1)\right)$ monotonically increases while $\lambda(1)$ increases.

Appendix A.4 Deceleration-to-acceleration operation

If the vehicle is decelerating at the current time, the abscissa of the extreme point of the quadratic function (26) is

$$-\frac{B_2(k)}{2A_2(k)} = \frac{\lambda(k)}{\omega_{L2}Mr}. \tag{A31}$$

We select two covariate variables $\lambda_1(k)$ and $\lambda_2(k)$ with corresponding control inputs of $F_{b,1}(k)$ and $F_{b,2}(k)$ and define the current time $k=1$ as the starting time of the prediction horizon. Given $\lambda_1(1) > \lambda_2(1)$, we recursively extrapolate to $\lambda_1(t_f)$ and $\lambda_2(t_f)$. At the starting time, $v_{x,1}(1) = v_{x,2}(1) = v_{x,0}$, so the corresponding optimal control inputs $\lambda_1(1)$ and $\lambda_2(1)$ are

$$F_{b,1}(1) = \frac{\lambda_1(1)}{\omega_{L2}Mr} > F_{b,2}(1) = \frac{\lambda_2(1)}{\omega_{L2}Mr}. \tag{A32}$$

According to (16), we have

$$\dot{v}_{x,1}(1) = -\frac{F_{b,1}(1)}{Mr} - C_r g\cos(\theta) < \dot{v}_{x,2}(1) = -\frac{F_{b,2}(1)}{Mr} - C_r g\cos(\theta). \tag{A33}$$

Therefore, at time $k=2$, the vehicle speed satisfies the following relationship:

$$v_{x,1}(2) < v_{x,2}(2). \tag{A34}$$

According to (22), at time $k=1$, the following relationship holds between $\dot{\lambda}_1(1)$ and $\dot{\lambda}_2(1)$:

$$\dot{\lambda}_1(1) = -[2\omega_{L1}F_{t,1}(1)^2 v_{x,1}(1) + 2\omega_{L3}(v_{x,1}(1) - v_{x,\mathrm{ref}}(1))] > \dot{\lambda}_2(1) = -[2\omega_{L1}F_{t,2}(1)^2 v_{x,2}(1) + 2\omega_{L3}(v_{x,2}(1) - v_{x,\mathrm{ref}}(1))]. \tag{A35}$$

Then, the following relationship holds between $\lambda_1(2)$ and $\lambda_2(2)$ at time $k=2$:

$$\lambda_1(2) = \lambda_1(1) + \dot{\lambda}_1(1)\mathrm{d}t > \lambda_2(2) = \lambda_2(1) + \dot{\lambda}_2(1)\mathrm{d}t. \tag{A36}$$

When the vehicle accelerates at $k=2$, we have

$$F_{t,1}(2) = -\frac{\lambda_1(2)}{\omega_{L1}Mrv_{x,1}(2)^2} < F_{t,2}(2) = -\frac{\lambda_2(2)}{\omega_{L1}Mrv_{x,2}(2)^2}. \tag{A37}$$

Then, we recursively obtain

$$\dot{v}_{x,1}(2) = \frac{F_{t,1}(2)}{Mr} - C_r g\cos(\theta) < \dot{v}_{x,2}(2) = \frac{F_{t,2}(2)}{Mr} - C_r g\cos(\theta). \tag{A38}$$

If the relationship between (A38) and (A33) is consistent, then the remaining recursive process until the terminal time is consistent with (A34)–(A36). At the terminal time, it can be obtained that

$$\lambda_1(t_f) > \lambda_2(t_f), v_{x,1}(t_f) < v_{x,2}(t_f). \tag{A39}$$

Therefore, it can be obtained that

$$J_{\lambda,1}\left(\lambda_1(1)\right) = \lambda_1(t_f) - 2\phi_L\left(v_{x,1}(t_f) - v_{x,\mathrm{ref}}(t_f)\right) > J_{\lambda,2}\left(\lambda_2(1)\right) = \lambda_2(t_f) - 2\phi_L\left(v_{x,2}(t_f) - v_{x,\mathrm{ref}}(t_f)\right). \tag{A40}$$

As the vehicle changes from decelerating to accelerating, $J_\lambda\left(\lambda_1(1)\right)$ monotonically increases with increasing $\lambda(1)$.

In addition to accelerating and decelerating, vehicles drive at constant speed. When switching between constant-speed driving, accelerating and decelerating, the derivation relationship is consistent with the starting times of the four operation conditions A.1–A.4, which will not cause reverse effects.

In summary, it has been proven that $\lambda\left(s_0\right)$ is monotonic within the feasible set $\lambda\left(s_0\right) \in [\Lambda_L, \Lambda_U]$.

Appendix B Proof of different signs at the endpoints of the feasible set

Here, we prove that $J_\lambda\left(s_0\right)$ has different signs at the endpoints of the $\lambda\left(s_0\right)$ feasible set through the method of contradiction. At time t, the recurrence relationship between $\lambda_{\max}(t)$ and $\lambda_{\min}(t)$ can be derived according to (22)

$$\lambda_{\max}(t+1) = \lambda_{\max}(t) - P(t)\mathrm{d}t, \tag{B1}$$

$$\lambda_{\min}(t+1) = \lambda_{\min}(t) - P(t)\mathrm{d}t. \tag{B2}$$

The specific form of $P(t)$ is

$$P(t) = 2\omega_{L1}F_t(s)^2 v_x(s) + 2\omega_{L3}\left(v_x(s) - v_{x,\mathrm{ref}}(s)\right). \tag{B3}$$

Given a covariate variable $\tilde{\lambda}(t)$, its corresponding state and control variables are $\{\tilde{v}_x(t), \tilde{F}_u(t)\}$, where $F_u(t)$ is the comprehensive control input formed by the combination of the driving force $F_t(t)$ and the braking force $F_b(t)$. We assume that at time $t = t_f$, $\tilde{\lambda}(t_f)$ satisfies

$$J_\lambda\left(\tilde{\lambda}(1)\right) = \tilde{\lambda}(t_f) - 2\phi_L\left(\tilde{v}_x(t_f) - v_{x,\mathrm{ref}}(t_f)\right) > 0. \tag{B4}$$

Because $2\phi_L\left(\tilde{v}_x(t_f) - v_{x,\mathrm{ref}}(t_f)\right)$ must be greater than its minimum value, we have

$$J_\lambda\left(\tilde{\lambda}(1)\right) > \tilde{\lambda}(t_f) - 2\phi_L\left(\tilde{v}_x(t_f) - v_{x,\mathrm{ref}}(t_f)\right) > -2\phi_L\max\left|\tilde{v}_x(t_f) - v_{x,\mathrm{ref}}(t_f)\right| = \tilde{\lambda}_{\min}(t_f). \tag{B5}$$

Therefore, deriving backward from $t = t_f$ to $t = 1$, we obtain the reverse relationship

$$\begin{aligned}&\tilde{\lambda}(t_f - 1) - \lambda_{\min}(t_f - 1) = \tilde{\lambda}(t_f) - \lambda_{\min}(t_f) + \left[\tilde{P}(t_f - 1) - P_{\min}(t_f - 1)\right]\mathrm{d}t\\ &> \lambda_{\min}(t_f) - \lambda_{\min}(t_f) + \left[\tilde{P}(t_f - 1) - P_{\min}(t_f - 1)\right]\mathrm{d}t = \left[\tilde{P}(t_f - 1) - P_{\min}(t_f - 1)\right]\mathrm{d}t > 0.\end{aligned} \tag{B6}$$

Similarly, at time $t = k - 1$, the following relationship holds:

$$\begin{aligned}&\tilde{\lambda}\left(k-1\right) - \lambda_{\min}\left(k-1\right) = \tilde{\lambda}(k) - \lambda_{\min}(k) + \left[\tilde{P}\left(k-1\right) - P_{\min}\left(k-1\right)\right]\mathrm{d}t\\ &> \lambda_{\min}(k) - \lambda_{\min}(k) + \left[\tilde{P}\left(k-1\right) - P_{\min}\left(k-1\right)\right]\mathrm{d}t = \left[\tilde{P}\left(k-1\right) - P_{\min}\left(k-1\right)\right]\mathrm{d}t > 0.\end{aligned} \tag{B7}$$

Progressive recursion yields $\tilde{\lambda}(1) > \lambda_{\min}(1) = \Lambda_L$, which contradicts $\tilde{\lambda}(1) = \Lambda_L$. Using the same method, we can prove that $J_\lambda\left(\Lambda_U\right) > 0$; therefore, it can be proven that $J_\lambda\left(s_0\right)$ has different signs at the endpoints of the feasible set of $\lambda\left(s_0\right)$.

Appendix C Robustness analysis of the back-stepping controller

This article presents lateral and longitudinal decoupling control of vehicles in the Frenet coordinate system. According to the lateral error equations (28) and (29), the tracking error of the vehicle's longitudinal speed will impact the effectiveness of the lateral controller. Therefore, it is necessary to analyze the robustness of the back-stepping controller under longitudinal speed tracking error. Assuming the tracking error of longitudinal vehicle speed is d, in the presence of error d, the error equations (28) and (29) become

$$\dot{e}_d(s) = \left(v_x(s) + d\right)e_\varphi(s), \tag{C1}$$

$$\dot{e}_\varphi(s) = \frac{v_r(s)}{L}\delta_f(s) - \kappa(s)\left(v_x(s) + d\right). \tag{C2}$$

Applying the lateral control input to the system of (C1) and (C2), the system becomes

$$\dot{e}_d(s) = (v_x(s) + d)\, e_\varphi(s), \tag{C3}$$

$$\dot{e}_\varphi(s) = -(K_1 + K_2)\, e_\varphi(s) - e_d(s)\,(v_x(s) + d)\,. \tag{C4}$$

Let the Lyapunov function of the system be

$$V = \frac{1}{2} e_d(s)^2 + \frac{1}{2} e_\varphi(s)^2. \tag{C5}$$

The derivative of the Lyapunov function (C5) is

$$\dot{V} = -(K_1 + K_2)\, e_\varphi(s)^2 \leqslant 0. \tag{C6}$$

Therefore, the error systems (C1) and (C2) are input state stable (ISS) relative to the error d, and the error system is robust to the longitudinal velocity tracking error considered.